Three-dimensional inversion of magnetotelluric data in complex geological structures

Michael S. Zhdanov and Nikolay Golubev
Department of Geology and Geophysics, University of Utah,
Salt Lake City, Utah

Abstract

Interpretation of magnetotelluric data over inhomogeneous geological structures is still a challenging problem in geophysical exploration. We have developed a new 3-D MT inversion method and a computer code based on full nonlinear conjugate gradient inversion and quasi-analytical approximation for forward modeling solution. Application of the QA approximation to forward modeling and Frechet derivative computations speeds up the calculation dramatically. However, in order to control the accuracy of the inversion, our method allows application of the rigorous forward modeling in the intermediate steps of the inversion procedure and for the final inverse model. The 3-D magnetotelluric inversion code QAINV3D based on QA approximation, has been tested on synthetic models and applied to the practical MT data collected in an area with complex geology. The inversion of 3-D MT data can be done within a few minutes on a PC to generate a 3-D image of subsurface formations on a large grid with tens of thousands of cells.

Introduction

Three-dimensional interpretation of array magnetotelluric data is an active area of the research and development conducted by the Consortium for Electromagnetic Modeling and Inversion (CEMI) at the University of Utah. In

recent years we have developed a new method of solving this problem using fast but accurate quasi-linear (QL) and quasi-analytical (QA) approximations for forward modeling solution (Zhdanov et. al., 2000a,b; Zhdanov and Hursan, 2000; Hursan and Zhdanov, 2001). The QA and QA approximations provide a fast and accurate tool for forward modeling that can be successfully used in inversion algorithms. At the final stage of the inversion we apply the rigorous forward modeling method to confirm the accuracy of our inversion result. This approach ensures the speed and efficiency of 3-D magnetotelluric inversion. However, the MT inversion technique developed in the previous publications was based on linearized expressions of the TE and TM mode impedances of the observed magnetotelluric field. In the current paper we present the results of the further development of this method. We introduce a method of 3-D inversion which does not use a linearized approach to constructing the forward modeling operator for MT data. The method is based on full nonlinear inversion using the re-weighted regularized conjugate gradient method developed by Zhdanov and Hursan (2000) and Zhdanov (2002). The main distinguishing feature of this algorithm is application of the special stabilization functionals which allow construction of both smooth images of the underground geoelectrical structures and models with sharp geoelectrical boundaries (Zhdanov, 2002). This approach to MT data inversion was first realized for 2-D inversion by Mehanee and Zhdanov (2002). We now extend it for full 3-D MT inversion. We also consider the full impedance tensor inversion of the MT data. The new fast 3-D MT inversion technique is applied to three-dimensional MT data collected by the INCO Exploration in Canada.

Inversion of the principal magnetotelluric impedances

The interpretation of magnetotelluric (MT) data is based on the calculation of the transfer functions between the horizontal components of the electric and magnetic fields according to the following formulae (Zhdanov and Keller, 1994; Berdichevsky and Dmitriev, 2002)

$$E_x = Z_{xx}H_x + Z_{xy}H_y, \tag{1}$$

$$E_y = Z_{yx}H_x + Z_{yy}H_y, \tag{2}$$

where $\{Z_{xx}, Z_{yy}, Z_{xy}, Z_{yx}\}$ are the components of the *impedance tensor* in some Cartesian coordinate system

$$\widehat{\mathbf{Z}} = \begin{bmatrix} Z_{xx} & Z_{xy} \\ Z_{yx} & Z_{yy} \end{bmatrix}.$$

In the general case, the solution of a 3-D magnetotelluric inverse problem has to be based on the simultaneous inversion of all four components of the impedance tensor. However, we consider first a simpler problem where only the principal impedances Z_{xy} and Z_{yx} are used for the inversion. The case of full impedance tensor inversion will be examined in the following sections.

The matrix form of the quasi-analytical (QA) approximation

In the framework of the QA approximation the anomalous electromagnetic field is expressed using the following integral representations (Zhdanov et al., 2000b)

$$\mathbf{E}^a(\mathbf{r}_j) \approx \mathbf{E}^a_{QA}(\mathbf{r}_j) = \int_D \widehat{\mathbf{G}}_E(\mathbf{r}_j \mid \mathbf{r}) \frac{\Delta\sigma(\mathbf{r})}{1 - g(\mathbf{r})} \mathbf{E}^b(\mathbf{r})\, dv, \tag{3}$$

$$\mathbf{H}^a(\mathbf{r}_j) \approx \mathbf{H}^a_{QA}(\mathbf{r}_j) = \int_D \widehat{\mathbf{G}}_H(\mathbf{r}_j \mid \mathbf{r}) \frac{\Delta\sigma(\mathbf{r})}{1 - g(\mathbf{r})} \mathbf{E}^b(\mathbf{r})\, dv. \tag{4}$$

Here $\widehat{\mathbf{G}}_E(\mathbf{r}_j \mid \mathbf{r})$ and $\widehat{\mathbf{G}}_H(\mathbf{r}_j \mid \mathbf{r})$ are the electric and magnetic Green's tensors defined for an unbounded conductive medium with the background conductivity σ_b, and function $g(\mathbf{r}_j)$ is the normalized dot product of the Born approximation, $\mathbf{E}^B$, and the background field, $\mathbf{E}^b$:

$$g(\mathbf{r}_j) = \frac{\mathbf{E}^B(\mathbf{r}_j) \cdot \mathbf{E}^{b*}(\mathbf{r}_j)}{\mathbf{E}^b(\mathbf{r}_j) \cdot \mathbf{E}^{b*}(\mathbf{r}_j)}, \text{ assuming } \mathbf{E}^b(\mathbf{r}_j) \cdot \mathbf{E}^{b*}(\mathbf{r}_j) \neq 0, \tag{5}$$

where "*" means complex conjugate vector.

The Born approximation is computed by the formula

$$\mathbf{E}^B(\mathbf{r}_j) = \int_D \widehat{\mathbf{G}}_E(\mathbf{r}_j \mid \mathbf{r})\, \Delta\sigma(\mathbf{r})\, \mathbf{E}^b(\mathbf{r})\, dv. \tag{6}$$

In practice we usually solve forward and inverse problems in the space of discrete data and model parameters. Suppose that L measurements of

an electric or magnetic field are performed in some electromagnetic experiment. Then we can consider these values as the components of electric, $\mathbf{e}$, or magnetic, $\mathbf{h}$, vectors of a length $3L$:

$$\mathbf{e} = [E_x^1, E_x^2, ...E_x^L, E_y^1, E_y^2, ...E_y^L, E_z^1, E_z^2, ...E_z^L]^T,$$

$$\mathbf{h} = [H_x^1, H_x^2, ...H_x^L, H_y^1, H_y^2, ...H_y^L, H_z^1, H_z^2, ...H_z^L]^T,$$

where the upper subscript "T" denotes a transpose operation of a vector row into a vector column.

Similarly, anomalous conductivity distribution, $\Delta\sigma(\mathbf{r})$, on some grid can be represented as the components of a vector $\mathbf{m}$ of the length N:

$$\mathbf{m} = [m_1, m_2, ..., m_N]^T = [\Delta\sigma_1, \Delta\sigma_2, ..., \Delta\sigma_N]^T.$$

Using these notations, we can write the discrete analogs of the quasi-analytical approximations (3) and (4), and the Born approximation (6), as (Zhdanov and Hursan, 2000):

$$\mathbf{e}_{QA}^a = \widehat{\mathbf{A}}_E \left[\mathbf{diag}\left(\mathbf{I}_N - \widehat{\mathbf{C}}\mathbf{m}\right)\right]^{-1} \mathbf{m} = \widehat{\mathbf{A}}_E \widehat{\mathbf{B}}(\mathbf{m})\ \mathbf{m},$$

$$\mathbf{h}_{QA}^a = \widehat{\mathbf{A}}_H \left[\mathbf{diag}\left(\mathbf{I}_N - \widehat{\mathbf{C}}\mathbf{m}\right)\right]^{-1} \mathbf{m} = \widehat{\mathbf{A}}_H \widehat{\mathbf{B}}(\mathbf{m})\ \mathbf{m}, \tag{7}$$

where $\widehat{\mathbf{A}}_E$ and $\widehat{\mathbf{A}}_H$ are the $3L \times N$ matrices

$$\widehat{\mathbf{A}}_E = \widehat{\mathbf{G}}_E \hat{\mathbf{e}}_D^b,\ \widehat{\mathbf{A}}_H = \widehat{\mathbf{G}}_H \hat{\mathbf{e}}_D^b, \tag{8}$$

and $\widehat{\mathbf{B}}(\mathbf{m})$ is the $N \times N$ diagonal matrix

$$\widehat{\mathbf{B}}(\mathbf{m}) = \left[\mathbf{diag}\left(\mathbf{I}_N - \widehat{\mathbf{C}}\mathbf{m}\right)\right]^{-1}, \tag{9}$$

where $\widehat{\mathbf{C}}$ is the $N \times N$ square matrix

$$\widehat{\mathbf{C}} = \left(\hat{\mathbf{e}}_D^b \hat{\mathbf{e}}_D^{b*}\right)^{-1} \hat{\mathbf{e}}_D^{b*} \widehat{\mathbf{G}}_D \hat{\mathbf{e}}_D^b. \tag{10}$$

We used the following notations in the last formulae. The vectors $\mathbf{e}^b$, $\mathbf{e}^a$, and $\mathbf{h}^a$ represent the discrete Born and quasi-analytical approximations of the anomalous electric field at the observation points. Matrix $\hat{\mathbf{e}}^b$ is a sparse tri-diagonal $3N \times N$ matrix containing the x, y and z components of the primary (background) electric field at the centers of the cells of the anomalous

domain D. Matrices $\widehat{\mathbf{G}}_E$ and $\widehat{\mathbf{G}}_H$ are discrete analogs of the corresponding Green's tensors. These matrices consist of the elements of either the electric or the magnetic Green's tensor acting from the anomalous body to the receivers. L is the number of receivers, and N is the number of cells in the anomalous body. Vector $\mathbf{I}$ is a column vector of the length N formed by units. Matrix $\widehat{\mathbf{G}}_D$ is a discrete analog of the corresponding electric Green's tensor acting inside the domain D (so-called *domain scattering matrix*). Appendix A contains the detailed explanation of these notations.

Let us introduce a notation $\mathbf{d}$ for an electric or magnetic vector of the anomalous part of the observed data. This vector contains the components of the anomalous electric and/or magnetic fields at the receivers. Using these notations, the forward modeling problem for the electromagnetic field can be expressed by the following matrix operation:

$$\mathbf{d} = \widehat{\mathbf{A}} \left[\mathbf{diag} \left(\mathbf{I} - \widehat{\mathbf{C}}\mathbf{m} \right) \right]^{-1} \mathbf{m} = \widehat{\mathbf{A}}\widehat{\mathbf{B}}(\mathbf{m})\, \mathbf{m}, \tag{11}$$

where $\widehat{\mathbf{A}}$ stands for the electric or magnetic matrices, $\widehat{\mathbf{A}}_E = \widehat{\mathbf{G}}_E \widehat{\mathbf{e}}^b$ or $\widehat{\mathbf{A}}_H = \widehat{\mathbf{G}}_H \widehat{\mathbf{e}}^b$, respectively.

TE and TM mode impedances in a 3-D magnetotelluric problem

In practice, the results of magnetotelluric measurements are usually presented as the apparent resistivity and phase calculated on the basis of the principal impedances, which are expressed as the ratio of the mutually orthogonal electric and magnetic field components (so-called nominal, TE and TM mode impedances, Zhdanov and Keller, 1994):

$$Z_{yx}^{TE} = E_y / H_x, \; Z_{xy}^{TM} = E_x / H_y. \tag{12}$$

Note that this 2-D nomenclature is artificial and approximate in nature for 3-D structures, because the TE and TM mode impedances, Z_{yx}^{TE} and Z_{xy}^{TM}, are not necessarily equal to the principal component of the full impedance tensors, Z_{yx} and Z_{xy}. However, it is widely used in practical MT observations. The model study shows that in many cases the difference between the nominal TE and TM mode impedances, Z_{yx}^{TE}, Z_{xy}^{TM}, and the principal components of the full impedance tensor, Z_{yx} , Z_{xy}, is negligibly small and does not affect the inversion result. The following numerical modelings illustrate this property

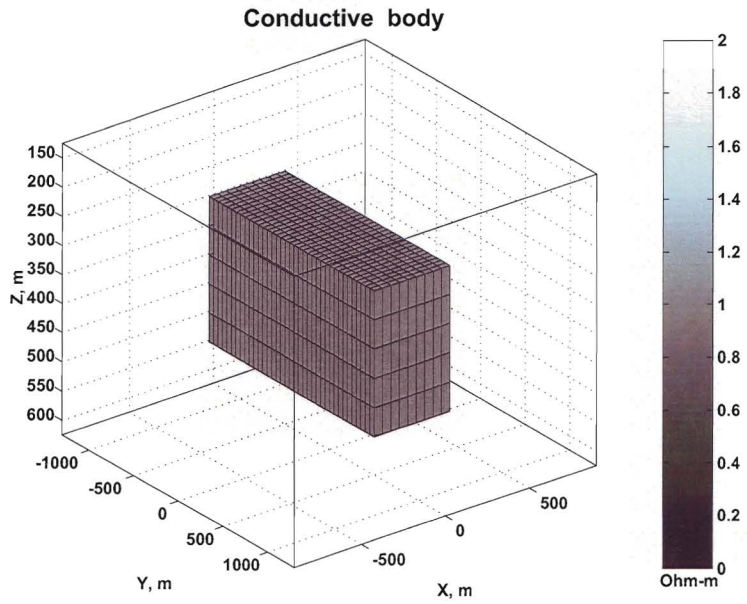

Figure 1: Model of conductive body. Resistivity of halfspace is 100 Ohmm. Resistivity of the anomaly is 10 Ohmm.

of the principal impedances. Figure 2 presents the Z_{yx} principal components of the full impedance tensor for the model of a conductive body shown in Figure 1. Figure 3 presents the difference between principal component Z_{yx} and the TE mode impedance Z_{yx}^{TE} for yx polarization. The amplitude of the difference is less than 1% of the amplitude of the component.

Figure 5 presents the same component for a more complex model of an elongated conductor oriented at an angle of 45 degrees with respect to the field polarization axes (Figure 4). The difference between these impedances is shown in Figure 6. The difference again is less than 1% of the component value.

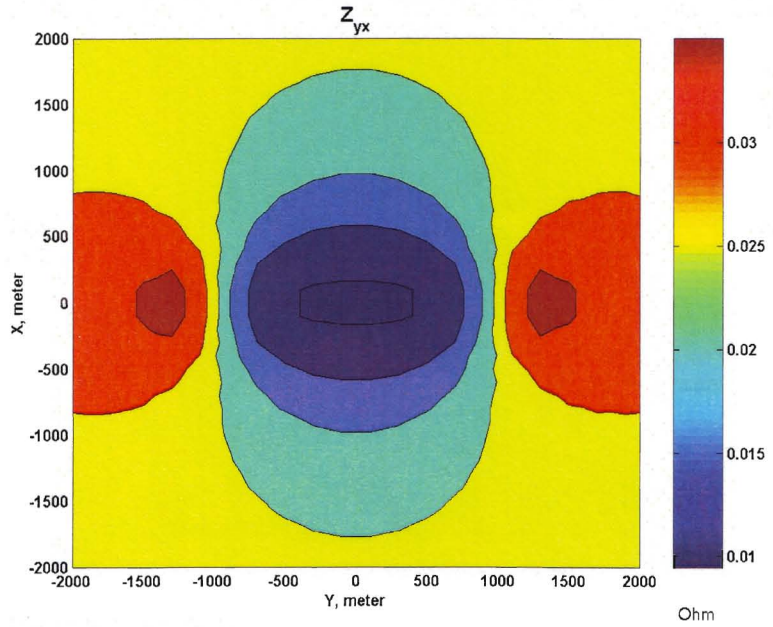

Figure 2: Principal component Z_{yx} of the full impedance tensor.

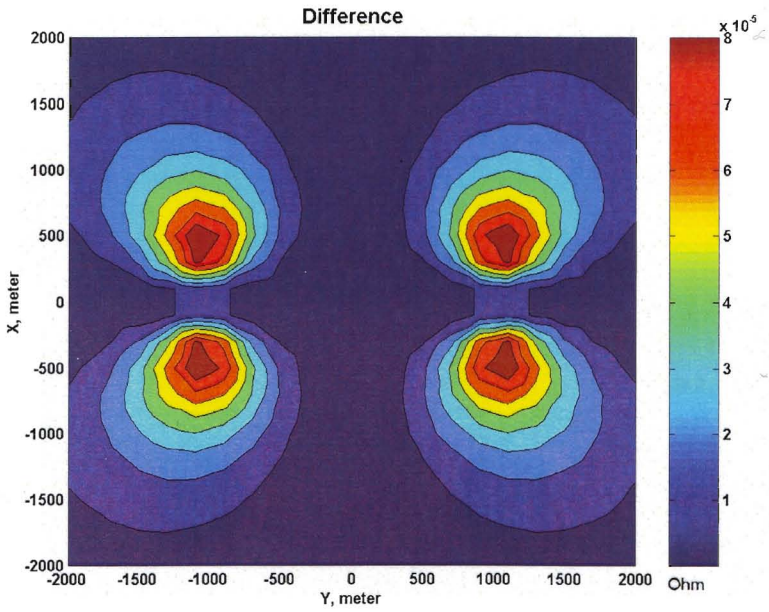

Figure 3: The difference between the principal component Z_{yx} and the TE mode impedance Z_{yx}^{TE} for yx polarization.

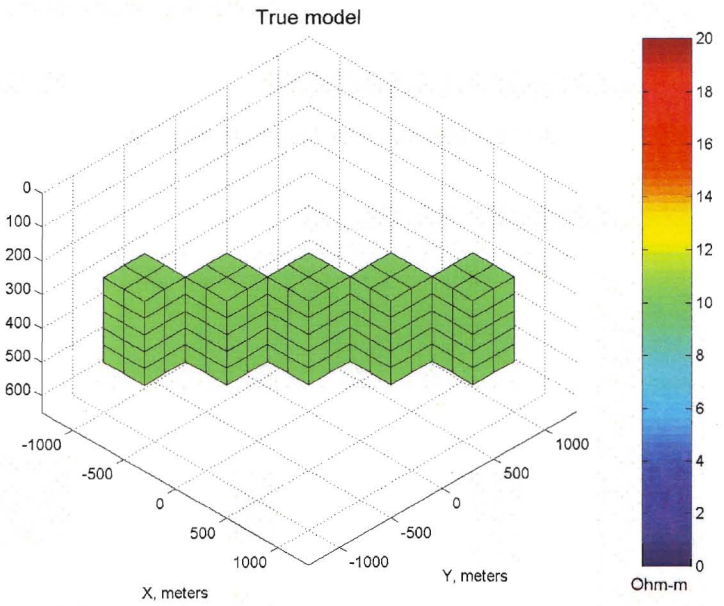

Figure 4: Model of diagonal conductive body.

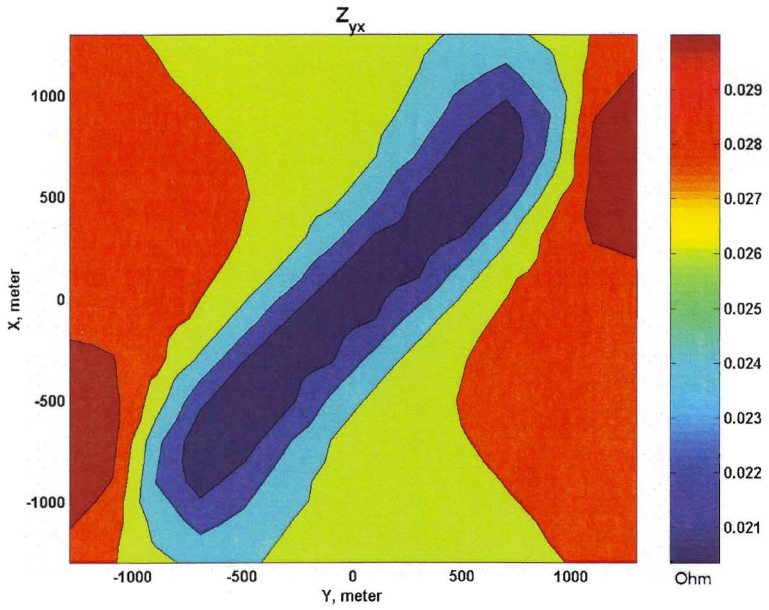

Figure 5: Principal component Z_{yx} of the full impedance tensor.

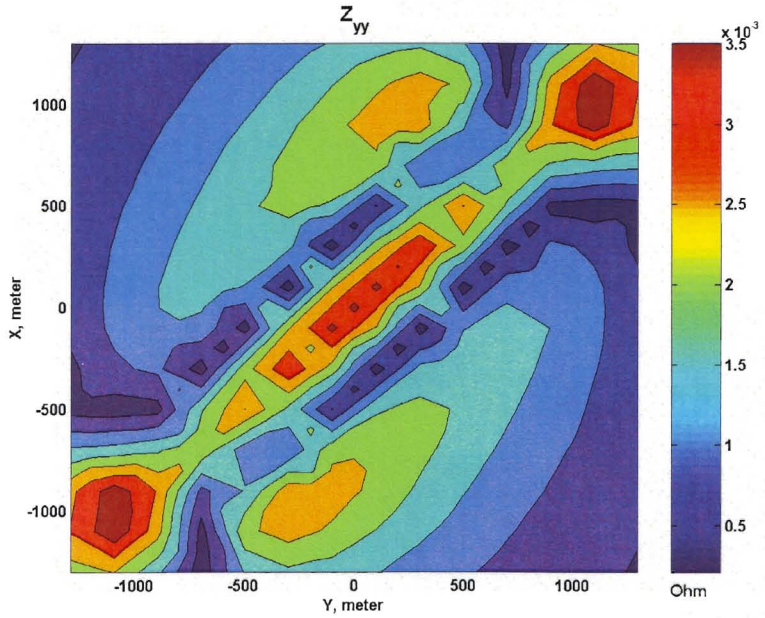

Figure 6: The difference between the principal component Z_{yx} and the TE mode impedance Z_{yx}^{TE} for yx polarization.

QA approximation of the TE and TM mode apparent resistivities and phases

Let us denote an arbitrary horizontal electric field component by E and define H as the magnetic field component perpendicular to the direction of E at a particular receiver site. Note that both E and H are complex numbers. The TE or TM mode magnetotelluric impedance is defined as the ratio of E and H :

$$Z = \frac{E}{H}. \tag{13}$$

The magnetotelluric apparent resistivity is calculated from Z, using

$$\rho = \frac{1}{\omega\mu_0}|Z|^2. \tag{14}$$

Formula (14) gives a nominal TE mode apparent resistivity if we use the TE mode impedance Z_{yx}^{TE}, and it produces a nominal TM mode apparent resistivity if we use the TM mode impedance Z_{xy}^{TM}. If the incident field is a plane-wave and the model is a homogeneous half-space, ρ is equal to the true resistivity, making it indicative of the resistivity structure of the subsurface.

Another commonly measured parameter is the phase angle of the impedance:

$$\phi = \tan^{-1}\frac{\mathrm{Im}Z}{\mathrm{Re}Z}. \tag{15}$$

This quantity is less sensitive to the effect of shallow subsurface anomalies, so it is particularly useful for the detection of deep structures.

To obtain a simple relationship between the anomalous field components and the MT parameters, let us express the logarithm of Z by writing $E = E^b + E^a$ and $H = H^b + H^a$:

$$\ln Z = \ln\frac{E^b + E^a}{H^b + H^a} = \ln\left(\frac{E^b + E^a}{E^b}\cdot\frac{H^b}{H^b + H^a}\cdot\frac{E^b}{H^b}\right). \tag{16}$$

Thus,

$$\ln Z = \ln\left(1 + E^a/E^b\right) - \ln\left(1 + H^a/H^b\right) + \ln Z^b, \tag{17}$$

where $Z^b = E^b/H^b$ is the *background impedance.*

From equation (14) we obtain

$$\ln|Z| = \ln\left[(\omega\mu_0\rho)^{1/2}\right] = \frac{1}{2}\ln(\omega\mu_0) + \frac{1}{2}\ln\rho. \tag{18}$$

The same relationship holds for the background impedance as well. Considering the identities $\ln Z = \ln|Z| + i\phi$ and $\ln Z^b = \ln|Z^b| + i\phi_b$ we find

$$\frac{1}{2}\ln\rho_a + i\phi_a = \ln\left(1 + E^a/E^b\right) - \ln\left(1 + H^a/H^b\right), \tag{19}$$

where $\ln\rho_a = \ln\rho - \ln\rho_b$ is the *log anomalous apparent resistivity*, and $\phi_a = \phi - \phi_b$ is the *anomalous phase*. Knowing the background cross-section, these quantities can be easily obtained from the measured total apparent resistivities and phases.

We introduce a vector of the data $\mathbf{d}^{MT}$, which combines the values of log-anomalous apparent resistivity at the receivers for all frequencies. In matrix notation, formula (19) is cast as

$$\mathbf{d}^{MT} = \frac{1}{2}\ln(\boldsymbol{\rho}^a) + i\boldsymbol{\phi}^a = \ln\left[\mathbf{I} + \left(\widehat{\mathbf{e}}^b\right)^{-1}\mathbf{e}^a\right] - \ln\left[\mathbf{I} + \left(\widehat{\mathbf{h}}^b\right)^{-1}\mathbf{h}^a\right], \tag{20}$$

where vector $\mathbf{I}$ is a $N \times 1$ column vector whose elements are all unity; $\widehat{\mathbf{e}}^b$ and $\widehat{\mathbf{h}}^b$ are diagonal matrices containing the background electric and magnetic fields at the receivers,

$$\widehat{\mathbf{e}}^b = \begin{bmatrix} E^{b,1} & & \\ & \ddots & \\ & & E^{b,N} \end{bmatrix}, \quad \widehat{\mathbf{h}}^b = \begin{bmatrix} H^{b,1} & & \\ & \ddots & \\ & & H^{b,N} \end{bmatrix}, \tag{21}$$

and it is assumed that ln is applied to each element of the corresponding vector.

Substituting the QA approximations (7) into the anomalous field components in (20), we obtain the QA approximation for the data containing the log anomalous apparent resistivities and phases:

$$\mathbf{d}^{MT} = \ln\left[\mathbf{I} + \left(\widehat{\mathbf{e}}^b\right)^{-1}\widehat{\mathbf{A}}_E\widehat{\mathbf{B}}(\mathbf{m})\mathbf{m}\right] - \ln\left[\mathbf{I} + \left(\widehat{\mathbf{h}}^b\right)^{-1}\widehat{\mathbf{A}}_H\widehat{\mathbf{B}}(\mathbf{m})\mathbf{m}\right], \tag{22}$$

where $\widehat{\mathbf{A}}_E = \widehat{\mathbf{G}}_E\widehat{\mathbf{e}}^b$ and $\widehat{\mathbf{A}}_H = \widehat{\mathbf{G}}_H\widehat{\mathbf{e}}^b$, respectively and

$$\widehat{\mathbf{B}}(\mathbf{m}) = \left[\mathbf{diag}\left(\mathbf{I} - \widehat{\mathbf{C}}\mathbf{m}\right)\right]^{-1}. \tag{23}$$

Thus, the MT inverse problem is reduced to the solution of the nonlinear matrix inverse problem (22).

Frechet derivative (sensitivity) matrix for log anomalous apparent resistivity and phase

Now let us consider the derivation of the Fréchet derivative matrix of the forward operator (22). Noting that the model parameters are the anomalous conductivity values in the cells of the anomalous body and that matrices $\widehat{\mathbf{C}}$, $\widehat{\mathbf{A}}_E$ and $\widehat{\mathbf{A}}_H$ are independent of the model parameters, one can express the perturbation of the forward operator (22) with respect to the model parameters in the form

$$\delta \mathbf{d}^{MT} = \left\{ \left(\widehat{\mathbf{e}}^b\right)^{-1} \widehat{\mathbf{A}}_E \mathbf{diag}^{-1} \left[\mathbf{I} + \left(\widehat{\mathbf{e}}^b\right)^{-1} \widehat{\mathbf{A}}_E \widehat{\mathbf{B}}(\mathbf{m})\mathbf{m}\right] \right.$$

$$\left. - \left(\widehat{\mathbf{h}}^b\right)^{-1} \widehat{\mathbf{A}}_H \mathbf{diag}^{-1} \left[\mathbf{I} + \left(\widehat{\mathbf{h}}^b\right)^{-1} \widehat{\mathbf{A}}_H \widehat{\mathbf{B}}(\mathbf{m})\mathbf{m}\right] \right\} \delta \left[\widehat{\mathbf{B}}(\mathbf{m})\mathbf{m}\right], \qquad (24)$$

where **diag** [...] means a diagonal matrix formed by the elements of the vector [...].

Since

$$\delta \left[\widehat{\mathbf{B}}(\mathbf{m})\right] = \delta \left[\mathbf{diag}\left(\mathbf{I} - \widehat{\mathbf{C}}\mathbf{m}\right)\right]^{-1}$$

$$= \left[\mathbf{diag}\left(\mathbf{I} - \widehat{\mathbf{C}}\mathbf{m}\right)\right]^{-2} \widehat{\mathbf{C}}\, \delta\mathbf{m} = \widehat{\mathbf{B}}^2(\mathbf{m})\, \widehat{\mathbf{C}}\, \delta\mathbf{m},$$

we obtain

$$\delta \left[\widehat{\mathbf{B}}(\mathbf{m})\ \mathbf{m}\right] = \left\{\widehat{\mathbf{B}}(\mathbf{m}) + \mathbf{diag}(\mathbf{m})\widehat{\mathbf{B}}^2(\mathbf{m})\ \widehat{\mathbf{C}}\right\} \delta\mathbf{m} = \widehat{\mathbf{D}}(\mathbf{m})\ \delta\mathbf{m}, \qquad (25)$$

where

$$\widehat{\mathbf{D}}(\mathbf{m}) = \widehat{\mathbf{B}}(\mathbf{m}) + \mathbf{diag}(\mathbf{m})\widehat{\mathbf{B}}^2(\mathbf{m})\ \widehat{\mathbf{C}} \qquad (26)$$

is a diagonal matrix.

Substituting expression (25) into (24), we find

$$\delta \mathbf{d}^{MT} = \left\{ \left(\widehat{\mathbf{e}}^b\right)^{-1} \widehat{\mathbf{A}}_E \mathbf{diag}^{-1} \left[\mathbf{I} + \left(\widehat{\mathbf{e}}^b\right)^{-1} \widehat{\mathbf{A}}_E \widehat{\mathbf{B}}(\mathbf{m})\mathbf{m}\right] \right.$$

$$\left. - \left(\widehat{\mathbf{h}}^b\right)^{-1} \widehat{\mathbf{A}}_H \mathbf{diag}^{-1} \left[\mathbf{I} + \left(\widehat{\mathbf{h}}^b\right)^{-1} \widehat{\mathbf{A}}_H \widehat{\mathbf{B}}(\mathbf{m})\mathbf{m}\right] \right\} \widehat{\mathbf{D}}(\mathbf{m})\ \delta\mathbf{m}.$$

From the last formula we find the MT Fréchet derivative matrix

$$\widehat{\mathbf{F}}^{MT}(\mathbf{m}) = \widehat{\mathbf{A}}^{MT}(\mathbf{m})\ \widehat{\mathbf{D}}(\mathbf{m}), \qquad (27)$$

where

$$\widehat{\mathbf{A}}^{MT}(\mathbf{m}) = \left(\widehat{\mathbf{e}}^b\right)^{-1} \widehat{\mathbf{A}}_E \mathbf{diag}^{-1} \left[\mathbf{I} + \left(\widehat{\mathbf{e}}^b\right)^{-1} \widehat{\mathbf{A}}_E \widehat{\mathbf{B}}(\mathbf{m})\mathbf{m}\right]$$

$$- \left(\widehat{\mathbf{h}}^b\right)^{-1}\widehat{\mathbf{A}}_H \mathbf{diag}^{-1}\left[\mathbf{I} + \left(\widehat{\mathbf{h}}^b\right)^{-1}\widehat{\mathbf{A}}_H\widehat{\mathbf{B}}(\mathbf{m})\mathbf{m}\right]. \tag{28}$$

Note that the terms depending on the model parameters are diagonal matrices. The full matrices, $\widehat{\mathbf{A}}_E$ and $\widehat{\mathbf{A}}_H$, depend only on the background conductivity distribution. Therefore, after precomputing the full matrices $\widehat{\mathbf{A}}_E$ and $\widehat{\mathbf{A}}_H$ for the background model, the iterative updating of $\widehat{\mathbf{F}}^{MT}(\mathbf{m})$ is relatively inexpensive during the inversion process.

Inversion of the full magnetotelluric impedance tensor

Calculating the components of the full impedance tensor

In the general case, solution of the inverse problem requires numerical modeling of the components of the full impedance tensor in each step of the iteration process. The simplest technique of solving this problem is outlined in Zhdanov and Keller (1994) and Berdichevsky and Dmitriev, 2002, and can be described as follows. We can write equation (1) for two polarizations of the background field,

$$\begin{aligned} E_x^{(1)} &= Z_{xx}H_x^{(1)} + Z_{xy}H_y^{(1)}, \\ E_x^{(2)} &= Z_{xx}H_x^{(2)} + Z_{xy}H_y^{(2)}, \end{aligned} \tag{29}$$

where the first case corresponds to the TM mode of the background field,

$$\mathbf{E}^{b(1)} = \left(E_x^{b(1)}, 0, 0\right), \ \mathbf{H}^{b(1)} = \left(0, H_y^{b(1)}, 0\right),$$

and the second case corresponds to the TE mode of the background field

$$\mathbf{E}^{b(2)} = \left(0, E_y^{b(2)}, 0\right), \ \mathbf{H}^{b(2)} = \left(H_x^{b(2)}, 0, 0\right).$$

Solving equations (29) with respect to the impedance tensor components Z_{xy} and Z_{xx}, we find

$$Z_{xy} = \frac{E_x^{(1)}H_x^{(2)} - E_x^{(2)}H_x^{(1)}}{H_y^{(1)}H_x^{(2)} - H_y^{(2)}H_x^{(1)}}, \ Z_{xx} = \frac{E_x^{(1)}H_y^{(2)} - E_x^{(2)}H_y^{(1)}}{H_x^{(1)}H_y^{(2)} - H_x^{(2)}H_y^{(1)}}. \tag{30}$$

In order to find the impedances Z_{yx} and Z_{yy}, we can write equation (2) for two polarizations of the background field as well and solve the resulting system of equations with respect to the impedance tensor components Z_{yy} and Z_{yx}:

$$Z_{yy} = \frac{E_y^{(1)} H_x^{(2)} - E_y^{(2)} H_x^{(1)}}{H_y^{(1)} H_x^{(2)} - H_y^{(2)} H_x^{(1)}}, \; Z_{yx} = \frac{E_y^{(1)} H_y^{(2)} - E_y^{(2)} H_y^{(1)}}{H_x^{(1)} H_y^{(2)} - H_x^{(2)} H_y^{(1)}}.$$

We can introduce the normalized impedances

$$Z_{xy}^n = Z_{xy}/Z_{xy}^b, \; Z_{xx}^n = Z_{xx}/Z_{xy}^b, \; Z_{yy}^n = Z_{yy}/Z_{yx}^b, \text{ and } Z_{yx}^n = Z_{yx}/Z_{yx}^b, \quad (31)$$

where

$$Z_{xy}^b = \frac{E_x^{b(1)}}{H_y^{b(1)}}, \; Z_{yx}^b = \frac{E_y^{b(2)}}{H_x^{b(2)}}. \quad (32)$$

In particular,

$$Z_{xy}^n = \frac{Z_{xy}}{Z_{xy}^b} = \frac{H_y^{b(1)}}{E_x^{b(1)}} \frac{E_x^{(1)} H_x^{(2)} - E_x^{(2)} H_x^{(1)}}{H_y^{(1)} H_x^{(2)} - H_y^{(2)} H_x^{(1)}}. \quad (33)$$

To obtain a simple relationship between the anomalous field components and the impedance tensor components, let us express the logarithm of Z by taking into account that

$$\mathbf{E}^{(1)} = \left(E_x^{(1)}, E_y^{a(1)}, E_z^{a(1)}\right), \; \mathbf{H}^{(1)} = \left(H_x^{a(1)}, H_y^{(1)}, H_z^{a(1)}\right),$$

$$\mathbf{E}^{(2)} = \left(E_x^{a(2)}, E_y^{(2)}, E_z^{a(2)}\right), \; \mathbf{H}^{(2)} = \left(H_x^{(2)}, H_y^{a(2)}, H_z^{a(2)}\right),$$

$$E_x^{(1)} = E_x^{a(1)} + E_x^{b(1)}, \; H_y^{(1)} = H_y^{a(1)} + H_y^{b(1)},$$

$$E_y^{(1)} = E_y^{a(1)}, \; H_x^{(1)} = H_x^{a(1)}, \; E_x^{(2)} = E_x^{a(2)}, \; H_y^{(2)} = H_y^{a(2)},$$

and

$$E_y^{(2)} = E_y^{a(2)} + E_y^{b(2)}, \; H_x^{(2)} = H_x^{a(2)} + H_x^{b(2)}.$$

As a result, we can write

$$\ln Z_{xy}^n = \ln Z_{xy} - \ln Z_{xy}^b = \ln \left\{ \left[\frac{E_x^{a(1)}}{E_x^{b(1)}} + 1 \right] \left[\frac{H_x^{a(2)}}{H_x^{b(2)}} + 1 \right] - \frac{E_x^{a(2)}}{H_x^{b(2)}} \frac{H_x^{a(1)}}{E_x^{b(1)}} \right\}$$

$$- \ln \left\{ \left[\frac{H_y^{a(1)}}{H_y^{b(1)}} + 1 \right] \left[\frac{H_x^{a(2)}}{H_x^{b(2)}} + 1 \right] - \frac{H_y^{a(2)}}{H_x^{b(2)}} \frac{H_x^{a(1)}}{H_y^{b(1)}} \right\}. \quad (34)$$

We can obtain similar expression for the log normalized impedance Z^n_{yx}:

$$\ln Z^n_{yx} = \ln Z_{yx} - \ln Z^b_{yx} = \ln\left\{\frac{E_y^{a(1)}}{H_y^{b(1)}}\frac{H_y^{a(2)}}{E_y^{b(2)}} - \left[\frac{E_y^{a(2)}}{E_y^{b(2)}}+1\right]\left[\frac{H_y^{a(1)}}{H_y^{b(1)}}+1\right]\right\}$$

$$-\ln\left\{\frac{H_x^{a(1)}}{H_y^{b(1)}}\frac{H_y^{a(2)}}{H_x^{b(2)}} - \left[\frac{H_x^{a(2)}}{H_x^{b(2)}}+1\right]\left[\frac{H_y^{a(1)}}{H_y^{b(1)}}+1\right]\right\}. \tag{35}$$

In a similar way, we can derive the normalized impedances $Z^n_{xx} = Z_{xx}/Z^b_{xy}$ and $Z^n_{yy} = Z_{yy}/Z^b_{yx}$.

Matrix representation of the impedance data

Let us organize the impedances into a data vector. For example, we introduce a vector $\mathbf{d}_{xy}$ formed by the values of the log impedance component $\ln Z^n_{xy}$ at L receivers

$$\begin{aligned}\mathbf{d}_{xy} = \ln\Big\{&\mathbf{diag}\left[\left(\widehat{\mathbf{e}}^{b(1)}\right)^{-1}\mathbf{e}_x^{a(1)}+\mathbf{I}_L\right]\left[\left(\widehat{\mathbf{h}}^{b(2)}\right)^{-1}\mathbf{h}_x^{a(2)}+\mathbf{I}_L\right]\\ &-\mathbf{diag}\left[\left(\widehat{\mathbf{h}}^{b(2)}\right)^{-1}\mathbf{e}_x^{a(2)}\right]\left(\widehat{\mathbf{e}}^{b(1)}\right)^{-1}\mathbf{h}_x^{a(1)}\Big\}\\ -\ln\Big\{&\mathbf{diag}\left[\left(\widehat{\mathbf{h}}^{b(1)}\right)^{-1}\mathbf{h}_y^{a(1)}+\mathbf{I}_L\right]\left[\left(\widehat{\mathbf{h}}^{b(2)}\right)^{-1}\mathbf{h}_x^{a(2)}+\mathbf{I}_L\right]\\ &-\mathbf{diag}\left[\left(\widehat{\mathbf{h}}^{b(2)}\right)^{-1}\mathbf{h}_y^{a(2)}\right]\left(\widehat{\mathbf{h}}^{b(1)}\right)^{-1}\mathbf{h}_x^{a(1)}\Big\},\end{aligned} \tag{36}$$

where $\mathbf{I}_L$ is a column vector of the order L formed by units; $\widehat{\mathbf{e}}^b$ and $\widehat{\mathbf{h}}^b$ are diagonal matrices containing the corresponding components of the background electric and magnetic fields at the receivers:

$$\widehat{\mathbf{e}}^{b(1)} = \begin{bmatrix} E_x^{b,1} & & \\ & \ddots & \\ & & E_x^{b,L}\end{bmatrix}, \quad \widehat{\mathbf{h}}^{b(1)} = \begin{bmatrix} H_y^{b,1} & & \\ & \ddots & \\ & & H_y^{b,L}\end{bmatrix},$$

$$\widehat{\mathbf{h}}^{b(2)} = \begin{bmatrix} H_x^{b,1} & & \\ & \ddots & \\ & & H_x^{b,L}\end{bmatrix}, \tag{37}$$

$$\mathbf{e}_x = [E_x^1, E_x^2, ...E_x^L]^T,$$

$$\mathbf{e}_y = [E_y^1, E_y^2, ...E_y^L]^T,$$
$$\mathbf{h}_x = [H_x^1, H_x^2, ...H_x^L]^T,$$
$$\mathbf{h}_y = [H_y^1, H_y^2, ...H_y^L]^T,$$

diag [...] means a diagonal matrix formed by the elements of the vector [...], and it is assumed that ln is applied to each element of the corresponding vector.

We express now the vectors $\mathbf{e}_x^a, \mathbf{e}_y^a, \mathbf{h}_x^a, \mathbf{h}_y^a$ using the QA approximations (7):

$$\mathbf{e}_x^a = \widehat{\mathbf{A}}_{E_x} \left[\mathbf{diag}\left(\mathbf{I}_N - \widehat{\mathbf{C}}\mathbf{m}\right)\right]^{-1} \mathbf{m} = \widehat{\mathbf{A}}_{E_x}\widehat{\mathbf{B}}(\mathbf{m})\ \mathbf{m},$$

$$\mathbf{h}_x^a = \widehat{\mathbf{A}}_{H_x} \left[\mathbf{diag}\left(\mathbf{I}_N - \widehat{\mathbf{C}}\mathbf{m}\right)\right]^{-1} \mathbf{m} = \widehat{\mathbf{A}}_{H_x}\widehat{\mathbf{B}}(\mathbf{m})\ \mathbf{m}, \tag{38}$$

$$\mathbf{e}_y^a = \widehat{\mathbf{A}}_{E_y} \left[\mathbf{diag}\left(\mathbf{I}_N - \widehat{\mathbf{C}}\mathbf{m}\right)\right]^{-1} \mathbf{m} = \widehat{\mathbf{A}}_{E_y}\widehat{\mathbf{B}}(\mathbf{m})\ \mathbf{m},$$

$$\mathbf{h}_y^a = \widehat{\mathbf{A}}_{H_y} \left[\mathbf{diag}\left(\mathbf{I}_N - \widehat{\mathbf{C}}\mathbf{m}\right)\right]^{-1} \mathbf{m} = \widehat{\mathbf{A}}_{H_y}\widehat{\mathbf{B}}(\mathbf{m})\ \mathbf{m}, \tag{39}$$

where $\widehat{\mathbf{A}}_{E_x}$ and $\widehat{\mathbf{A}}_{H_x}$ are formed by the first L rows of matrices $\widehat{\mathbf{A}}_E$ and $\widehat{\mathbf{A}}_H$, while $\widehat{\mathbf{A}}_{E_y}$ and $\widehat{\mathbf{A}}_{H_y}$ are formed by the second L rows of matrices $\widehat{\mathbf{A}}_E$ and $\widehat{\mathbf{A}}_H$, respectively. In order to simplify the notations, we introduce a vector $\mathbf{P}(\mathbf{m})$

$$\mathbf{P}(\mathbf{m}) = \widehat{\mathbf{B}}(\mathbf{m})\ \mathbf{m}\ , \tag{40}$$

and denote matrices $\widehat{\mathbf{A}}_E$ and $\widehat{\mathbf{A}}_H$ by symbols $\widehat{\mathbf{E}}$ and $\widehat{\mathbf{H}}$ as follows:

$$\widehat{\mathbf{A}}_{E_{x,y}} = \widehat{\mathbf{E}}_{x,y},\ \widehat{\mathbf{A}}_{H_{x,y}} = \widehat{\mathbf{H}}_{x,y}, \tag{41}$$

Using these notations, we can express the vectors of the anomalous electric and magnetic fields in (38) and (39) as

$$\mathbf{e}_{x,y}^a = \widehat{\mathbf{E}}_{x,y}\mathbf{P}(\mathbf{m}),\ \mathbf{h}_{x,y}^a = \widehat{\mathbf{H}}_{x,y}\mathbf{P}(\mathbf{m}), \tag{42}$$

where $\widehat{\mathbf{E}}_{x,y}$ and $\widehat{\mathbf{H}}_{x,y}$ are $L \times N$ matrices independent of the model parameters $\mathbf{m}$, and $\mathbf{P}(\mathbf{m})$ is the column vector of the order N dependent on $\mathbf{m}$.

Substituting the QA approximations (42) into the anomalous field components in (36), we obtain the QA forward approximation for the data containing the log impedance Z_{xy}:

$$\mathbf{d}_{xy} = \ln\left\{\mathbf{diag}\left[\widehat{\mathbf{E}}_x^{e(1)}\mathbf{P}^{(1)}(\mathbf{m}) + \mathbf{I}_L\right]\left[\widehat{\mathbf{H}}_x^{h(2)}\mathbf{P}^{(2)}(\mathbf{m}) + \mathbf{I}_L\right]\right.$$

$$-\mathbf{diag}\left[\widehat{\mathbf{E}}_x^{h(2)}\mathbf{P}^{(2)}(\mathbf{m})\right]\widehat{\mathbf{H}}_x^{e(1)}\mathbf{P}^{(1)}(\mathbf{m})\Big\}$$

$$-\ln\Big\{\mathbf{diag}\left[\widehat{\mathbf{H}}_y^{h(1)}\mathbf{P}^{(1)}(\mathbf{m})+\mathbf{I}_L\right]\left[\widehat{\mathbf{H}}_x^{h(2)}\mathbf{P}^{(2)}(\mathbf{m})+\mathbf{I}_L\right]$$

$$-\mathbf{diag}\left[\widehat{\mathbf{H}}_y^{h(2)}\mathbf{P}^{(2)}(\mathbf{m})\right]\widehat{\mathbf{H}}_x^{h(1)}\mathbf{P}^{(1)}(\mathbf{m})\Big\}, \tag{43}$$

where indices (1) or (2) correspond to the TM or TE modes of the background field, and we use the notation

$$\left(\widehat{\mathbf{e}}^b\right)^{-1}\widehat{\mathbf{E}}_{x,y}=\widehat{\mathbf{E}}_{x,y}^e,\ \left(\widehat{\mathbf{h}}^b\right)^{-1}\widehat{\mathbf{H}}_{x,y}=\widehat{\mathbf{H}}_{x,y}^h,$$

$$\left(\widehat{\mathbf{h}}^b\right)^{-1}\widehat{\mathbf{E}}_{x,y}=\widehat{\mathbf{E}}_{x,y}^h,\ \left(\widehat{\mathbf{e}}^b\right)^{-1}\widehat{\mathbf{H}}_{x,y}=\widehat{\mathbf{H}}_{x,y}^e. \tag{44}$$

Using similar matrix representations for the anomalous electric and magnetic fields, we can write the corresponding expressions for vector $\mathbf{d}_{yx}$, $\mathbf{d}_{xx,}$, and $\mathbf{d}_{yy}$, formed by the values of the log impedance components $\ln Z_{yx}^n$, $\ln Z_{xx}^n$, and $\ln Z_{yy}^n$, at L receivers, respectively.

For example,

$$\mathbf{d}_{yx}=\ln\Big\{\mathbf{diag}\left[\widehat{\mathbf{E}}_y^{h(1)}\mathbf{P}^{(1)}(\mathbf{m})\right]\widehat{\mathbf{H}}_y^{e(2)}\mathbf{P}^{(2)}(\mathbf{m})$$

$$-\mathbf{diag}\left[\widehat{\mathbf{E}}_y^{e(2)}\mathbf{P}^{(2)}(\mathbf{m})+\mathbf{I}_L\right]\left[\widehat{\mathbf{H}}_y^{h(1)}\mathbf{P}^{(1)}(\mathbf{m})+\mathbf{I}_L\right]\Big\}$$

$$-\ln\Big\{\mathbf{diag}\left[\widehat{\mathbf{H}}_y^{h(2)}\mathbf{P}^{(2)}(\mathbf{m})\right]\widehat{\mathbf{H}}_x^{h(1)}\mathbf{P}^{(1)}(\mathbf{m})$$

$$-\mathbf{diag}\left[\widehat{\mathbf{H}}_y^{h(1)}\mathbf{P}^{(1)}(\mathbf{m})+\mathbf{I}_L\right]\left[\widehat{\mathbf{H}}_x^{h(2)}\mathbf{P}^{(2)}(\mathbf{m})+\mathbf{I}_L\right]\Big\}, \tag{45}$$

Thus, the MT inverse problem is reduced to the solution of the nonlinear matrix inverse problem, described by equations (43) - (45).

Note that expressions (43) - (45) can be used for calculating the Frechet derivative (sensitivity) matrix for the data formed by the full magnetotelluric (MT) impedance as well. The corresponding Frechet derivative matrix can be found similar to Frechet derivative calculation for apparent resistivity and phase, outlined above.

Regularized smooth and focusing inversion of MT data

The MT inverse problems described by the matrix nonlinear equations (22) and (43) - (45) are ill-posed problems. The solution of these problems requires the application of the corresponding regularization methods (Tikhonov

and Arsenin, 1977; Zhdanov, 2002). The traditional way to implement regularization in the solution of the inverse problem is based on a consideration of the class of inverse models with a smooth distribution of the model parameters. Within the framework of classical Tikhonov regularization, one can select a smooth solution by introducing the corresponding minimum norm, or "smoothing" stabilizing functionals. This approach is widely used in geophysics and has proven to be a powerful tool for stable inversion of geophysical data.

The traditional inversion algorithms providing smooth solutions for geoelectrical structures have difficulties, however, in describing the sharp geoelectrical boundaries between different geological formations. This problem arises, for example, in inversion for the local conductive target with sharp boundaries between the conductor and the resistive host rocks, which is a typical model in mining exploration. In these situations, it can be useful to search for a stable solution within the class of inverse models with sharp geoelectrical boundaries. The mathematical technique for solving this problem was described in Zhdanov and Hursan (2000) and Zhdanov (2002). It is based on introducing a special type of stabilizing functional, the so-called minimum support or minimum gradient support functionals (Portniaguine and Zhdanov, 1999; Mehanee and Zhdanov, 2002). We call this technique a focusing regularized inversion to distinguish it from the traditional smooth regularized inversion.

We can use the re-weighted regularized conjugate gradient (RRCG) method to solve the nonlinear inverse problems (22) and (43) - (45). The basic principles of the RRCG method are outlined in Zhdanov (2002). This method can incorporate both the smooth regularized inversion, which generates a smooth image of the inverted conductivity, and a focusing regularized inversion, producing a sharp focused image of the geoelectrical target.

Note that the total conductivity must always be positive in the predicted model. That is why we use the logarithm of the total conductivity as a model parameter ensuring realistic inverse models:

$$\widetilde{\mathbf{m}} = ln(\sigma_b + \mathbf{m}). \tag{46}$$

Obviously, this model parameter can never produce negative conductivity. The inverse transform is

$$\mathbf{m} = exp(\widetilde{\mathbf{m}}) - \sigma_b. \tag{47}$$

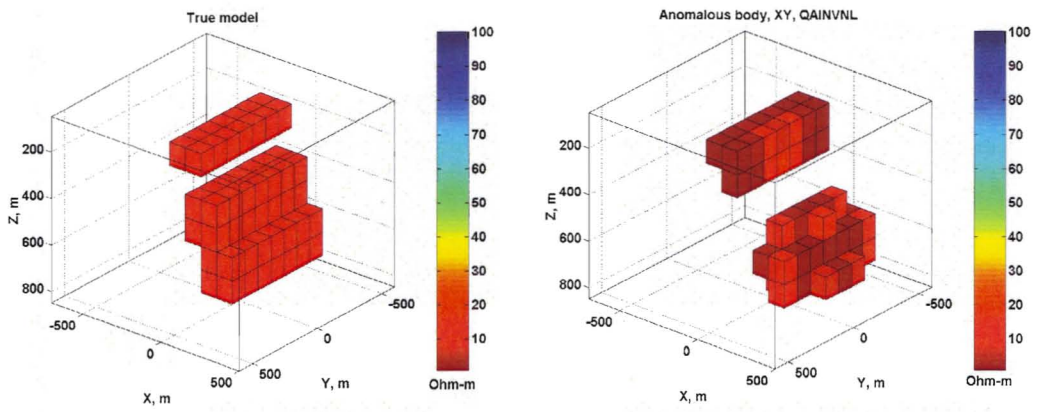

Figure 7: A model of a dipping dike (left panel) and inversion results obtained by the QA inversion method with focusing (right panel).

Model study

The synthetic MT data set is generated by the forward modeling code INTEM3D (Hursán and Zhdanov, 2002), based on the contraction integral equation method, for a model of a dipping dike (Figure 7, left panel) of resistivity 10 ohm-m, submerged in a half-space of 100 ohm-m. The top of the dike is at depth 200 m, and its bottom is at depth 700 m beneath the surface. The dike consists of two separated parts.

This model is excited by plane EM waves with four different frequencies: 1, 10, 100 and 1000 Hz. The MT impedances were calculated in 195 receivers placed on the nodes of a square grid on the surface. The distance between the observation points is 100 m in the x and y directions.

The volume of inversion is covered by a homogeneous mesh consisting of $15\times13\times8$ cubic cells surrounding the anomalous structure to be inverted. Each cell has a dimension of 100 m in the x, y and z directions. The region of inversion is also shown in Figure 7 (left and right panels).

The synthetic data set, generated by a full integral equation method, has been contaminated by 3 percent random noise. The model parameters are the unknown anomalous conductivity values of each cell in the volume over which the inversion is carried out.

It has been demonstrated by Wannamaker (1999) that the best results

for elongated anomalies are obtained with TM mode. The anomalous body has a strike along the y axis, so the TM mode corresponds to xy polarization (E_x and H_y). In the case of the TE mode, the primary electric field is polarized along the strike direction, and therefore, it is less sensitive to the dike boundaries parallel to the strike. In the case of the TM mode, the primary electric field is directed across the strike, and it becomes more sensitive to the dike boundaries.

Figure 7 presents the result of inversion for an TM mode impedance Z_{xy} using the quasi-analytical (QA) inversion method, with focusing. Note that inversion of theoretical MT data takes just few minutes on a personal computer. A remarkable fact is that it is possible for this polarization to separate the upper and lower parts of the dike. The position, shape, and ther resistivity of the dike are also reconstructed quite well.

The next model represents in a schematic way a conductive syncline type formation (Figure 8). We call this model an "open box" model. The conductive syncline has a resistivity of 10 Ohm-m, and the resistivity of the background is of 100 Ohm-m. The top of the conductor is at a depth of 200 m, and its bottom is at a depth of 1,100 m beneath the surface. The horizontal size of the conductor is 3,200 m by 2,000 m. The thickness of the "bottom" and the sides of the conductor is of 100 m. The horizontal cross-sections of the model at the different depths are shown in Figure 9. This model is excited by plane EM waves with four different frequencies: 0.1, 1, 10 and 100 Hz. The volume of inversion is covered by a homogeneous mesh consisting of $61\times41\times9$ cubic cells surrounding the anomalous structure to be inverted. Each cell has a dimension of 100 m in the x, y, and in the z directions. The synthetic data set is generated by the IE modeling code INTEM3D.

Figure 10 presents the result of inversion for the Z_{xy} impedance data using the quasi-analytical inversion with image focusing. The inversion result for the Z_{yx} impedance data is shown in Figure 11. One can see that, by using the different off-diagonal impedances, we can see better the different sides of the syncline. Figure 12 presents the result of the joint inversion of the off-diagonal impedances, Z_{xy} and Z_{yx}. This image reconstructs all sides of the conductor, however, the "open box" like model is slightly distorted in this case. One can see that a simple superposition of two models obtained for different off-diagonal impedances, produces better result then the joint inversion in this case.

The model study illustrates that in the case of a complex geological struc-

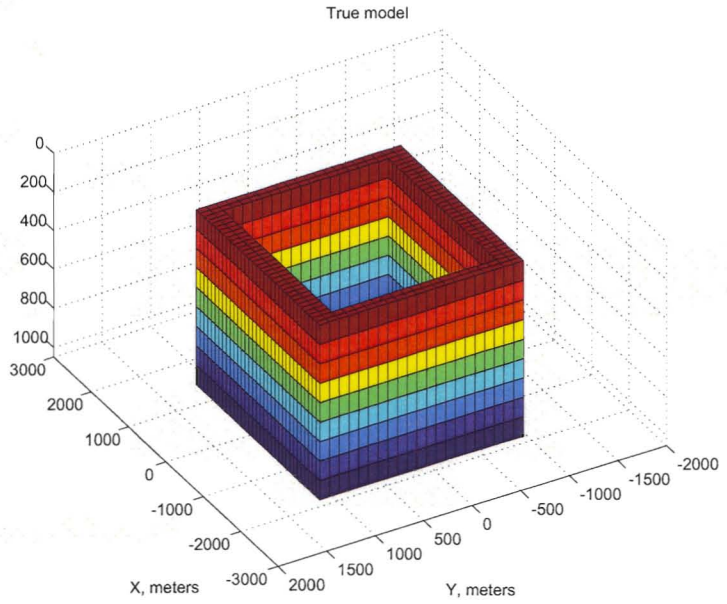

Figure 8: Volume image of the model of a conductive syncline type formation (an "open box" model). The color represents the depth of the corresponding cells: the shallow cells are marked by red, while the deep cells are painted in blue, for better visualization purpose.

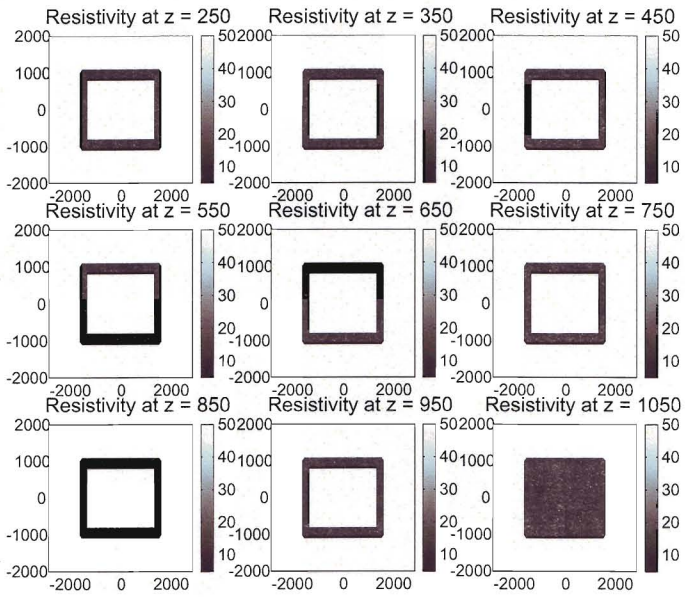

Figure 9: Horizontal slices of the model of a conductive syncline type formation at the different depths. The black&white scale represents the resistivity in Ohm-m.

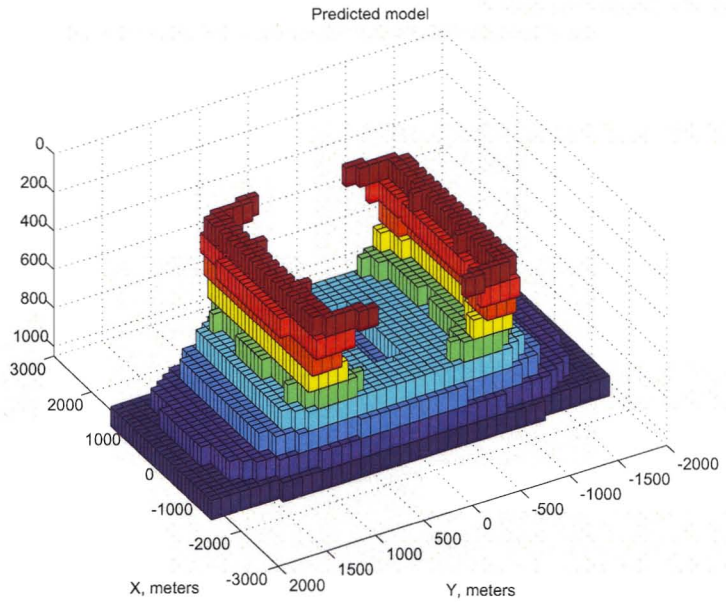

Figure 10: A volume rendering of the resistivity model obtained as result of the tensor component Z_{xy} quasi-analytical inversion (Model 3). The cut-off level for this image is equal to 15 Ohm-m. This means that only the cells with a value of resistivity less than 15 Ohm-m are displayed. The color represents the depth of the corresponding cells: the shallow cells are marked by red, while the deep cells are painted in blue.

ture, the joint inversion may be preferable, however, the individual inversion of a different impedance tensor component may contain complimentary information about the complex geological structure.

Inversion of the Voisey's Bay MT data

INCO Exploration conducted a three-dimensional MT survey. The goal of this survey was to study the application of the MT method to typical Ni-Cu-Fe sulphide mineralization zone exploration in complex geological structures. An array magnetotelluric survey consists of eleven profiles covering an area of about 28 km^2, collected by INCO Exploration at the Voisey's Bay area,

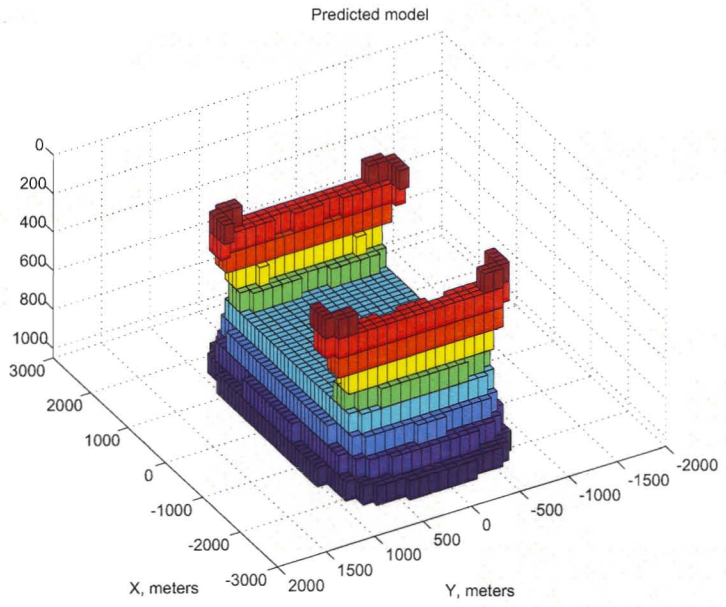

Figure 11: A volume rendering of the resistivity model obtained as a result of the tensor component Z_{yx} quasi-analytical inversion (Model 3). The cut-off level for this image is equal to 15 Ohm-m. The color represents the depth of the corresponding cells: the shallow cells are marked by red, while the deep cells are painted in blue.

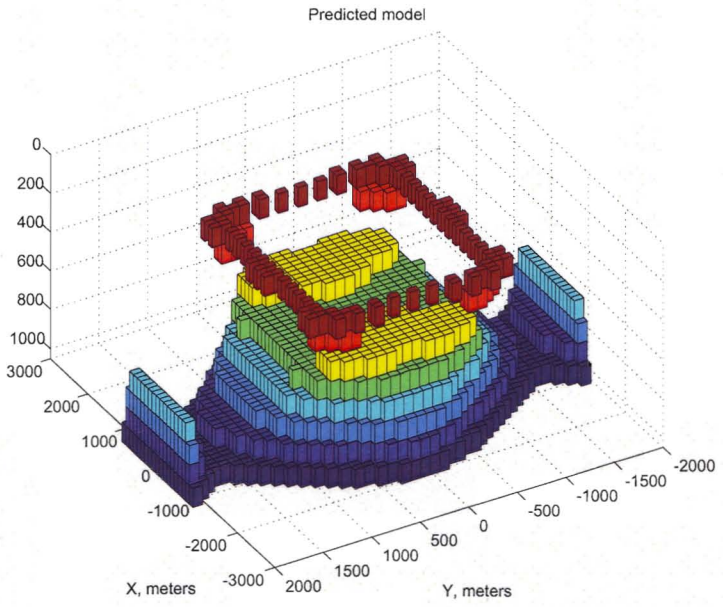

Figure 12: A volume rendering of the resistivity model obtained as a result of the joint inversion of off-diagonal tensor components Z_{xy} and Z_{yx} using the quasi-analytical inversion method with image focusing (Model 3). The cut-off level for this image is equal to 15 Ohm-m. The color represents the depth of the corresponding cells: the shallow cells are marked by red, while the deep cells are painted in blue.

where massive sulfide deposits were discovered (Naldrett et al., 1996; Balch, 2000). The frequency range of MT data is from 10 Hz to 350 Hz. We use for inversion two off-diagonal elements of the impedance tensor, Z_{xy} and Z_{yx}, at five different frequencies between 32 Hz and 288 Hz (288 Hz, 166 Hz, 95 Hz, 55 Hz, and 32 Hz). The diagonal components of the impedance tensor, Z_{xx} and Z_{yy}, were not used in the inversion because they were typically much smaller and noisier than the off-diagonal components (similar to the model case discussed above). The simple analysis of the MT data showed the presence of an anomaly zone between profiles number six and eleven. The MT profiles are numbered from the left to the right in Figure 13. For example, Figure 13 presents the maps of Z_{yx} apparent resistivity (top panel) and phase (bottom panel) for a frequency of 96 Hz. We can see clearly the location of the anomalous zone in these maps.

For detailed investigation we used data from the six profiles in the eastern part crossing the anomalous zone. The background geoelectrical cross-section in this area, according to the MT data, was represented by a seven-layer model with the following resistivity-sequence: $\rho_1 = 305$, $\rho_2 = 283$, $\rho_3 = 452$, $\rho_4 = 461$, $\rho_5 = 607$, $\rho_6 = 452$, $\rho_7 = 556$ Ohm-m; $h_1 = 100$, $h_2 = 200$, $h_3 = 200$, $h_4 = 100$, $h_5 = 100$, $h_6 = 200$ m. This cross-section has been found using the parameter-estimation code developed by Portniaguine and Zhdanov (1995). The area of inversion consists of 33600 ($56 \times 50 \times 12$) cells. Figure 14 presents the 3-D view of the area of inversion and its discretization. The structure of the MT station locations is a little bit irregular. The MT data were interpolated in the six profiles shown in Figure 14.

The rapid 3-D MT inversion method was applied to the off-diagonal MT impedances for the 276 interpolated MT soundings at five frequencies.

As a result of the inversion, we obtained a volume distribution of electrical resistivity under the area of about 28 km^2 to a depth of 1 km. In Figure 15a we can see the vertical cross-sections of the inverse results below the observation profiles. Figure 15b presents the general 3-D view of the predicted model. Figure 16 upper panel shows 3-D conductive bodies with resistivity below 25 ohm-m, while Figure 16 bottom panel presents the domains with resistivity below 50 ohm-m. One can see a conductive anomaly with a complex shape in Figure 16, reaching a depth of several hundred meters. We have plotted also the horizontal map at the different depths of the resistivity obtained as the result of the inversion. These maps are generated using the Geosoft package. An example of this map at a depth of 550 m is shown in Figure 17.

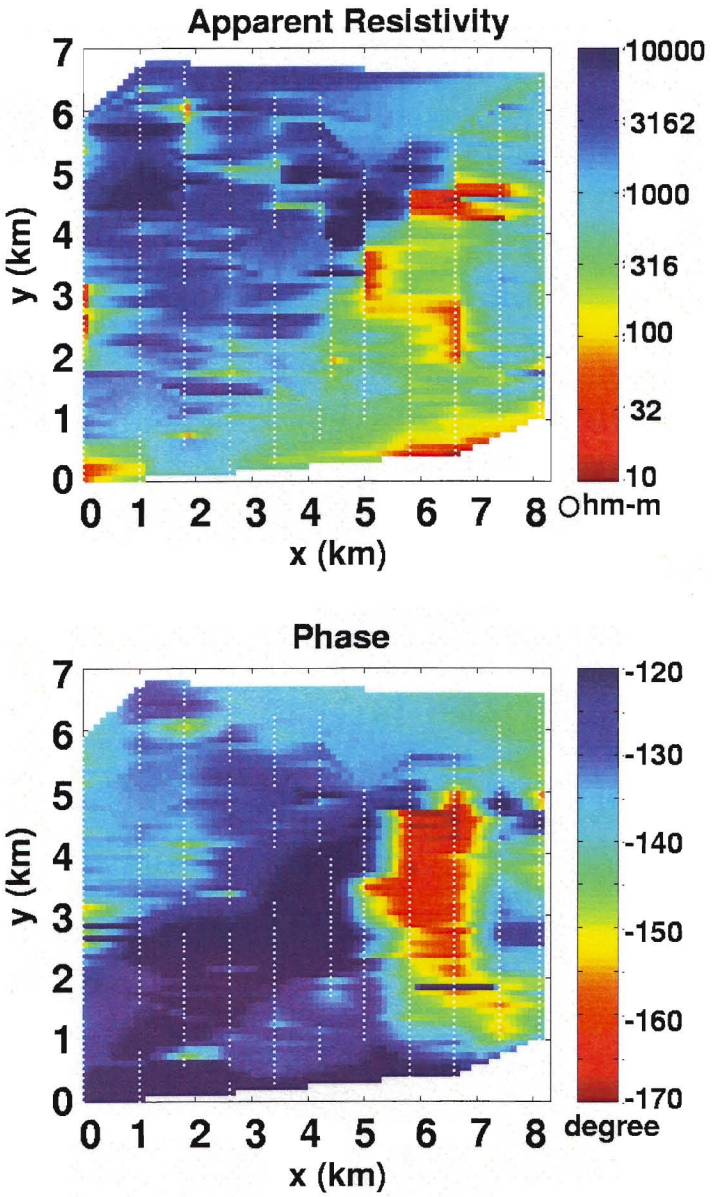

Figure 13: Maps of the observed Z_{yz} apparent resistivities and phases at f = 95 Hz over the Voisey's Bay area. The dots mark the observation sites.

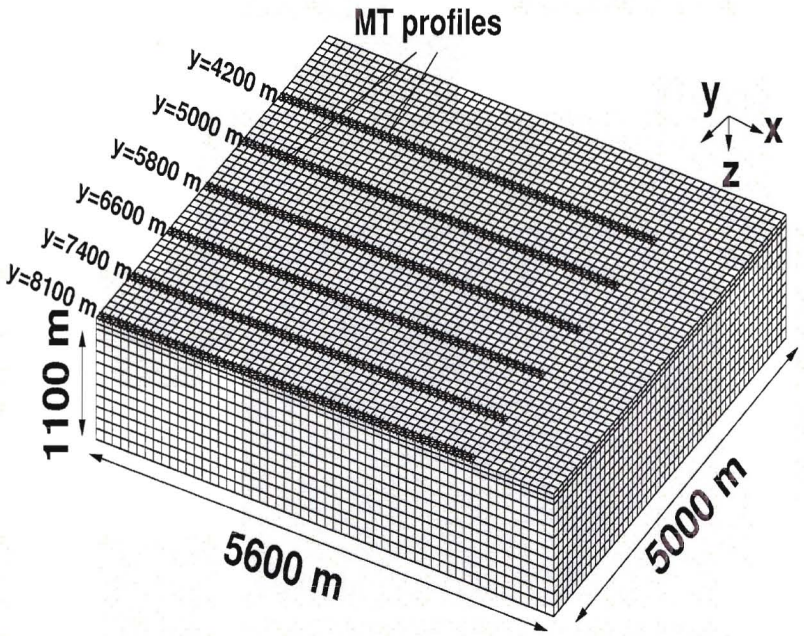

Figure 14: Three-dimensional sketch of the inverted area and its discretization for the inversion of the Voisey's Bay area data. The locations of the MT profiles are marked by thick black lines.

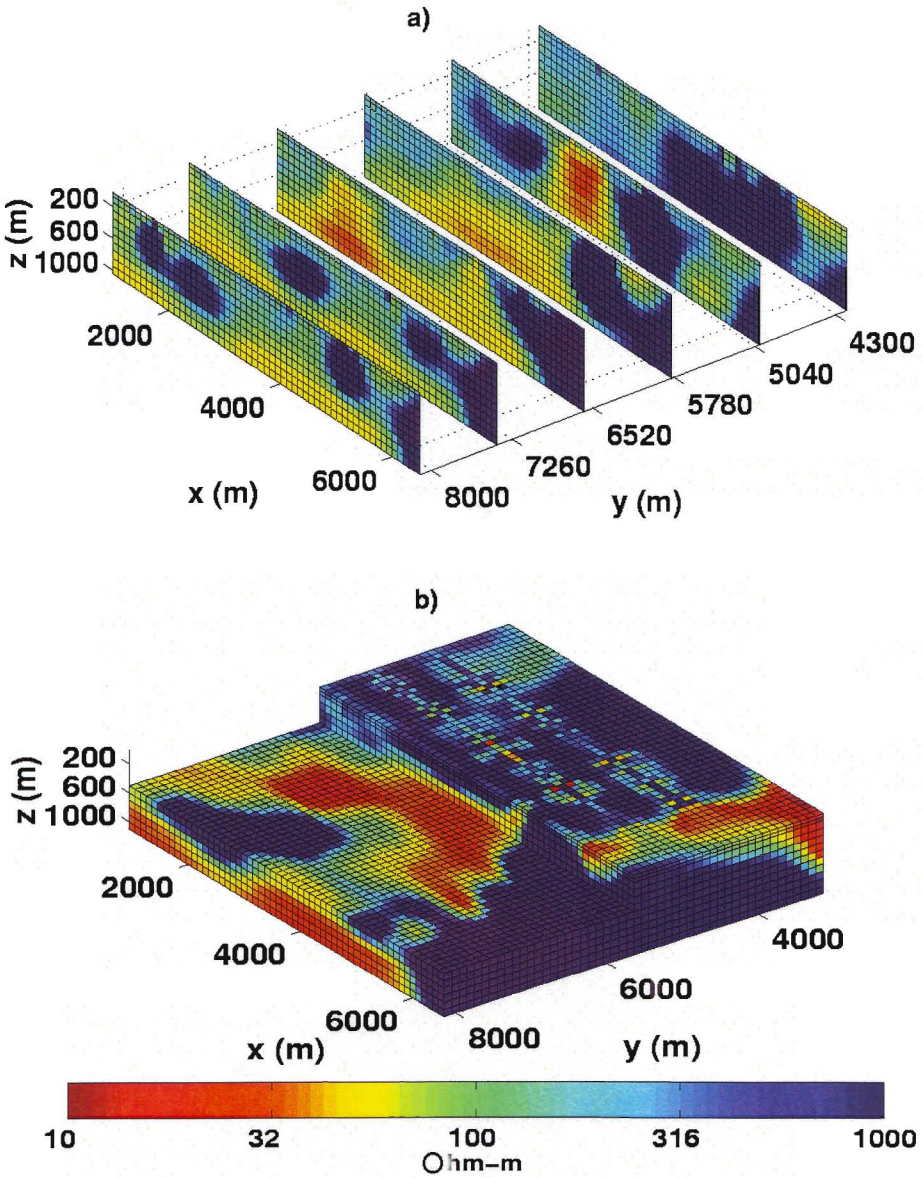

Figure 15: a) Vertical cross-sections and b) volume image of the predicted inverse resistivity model obtained by QA inversion of the Voisey's Bay area data set.

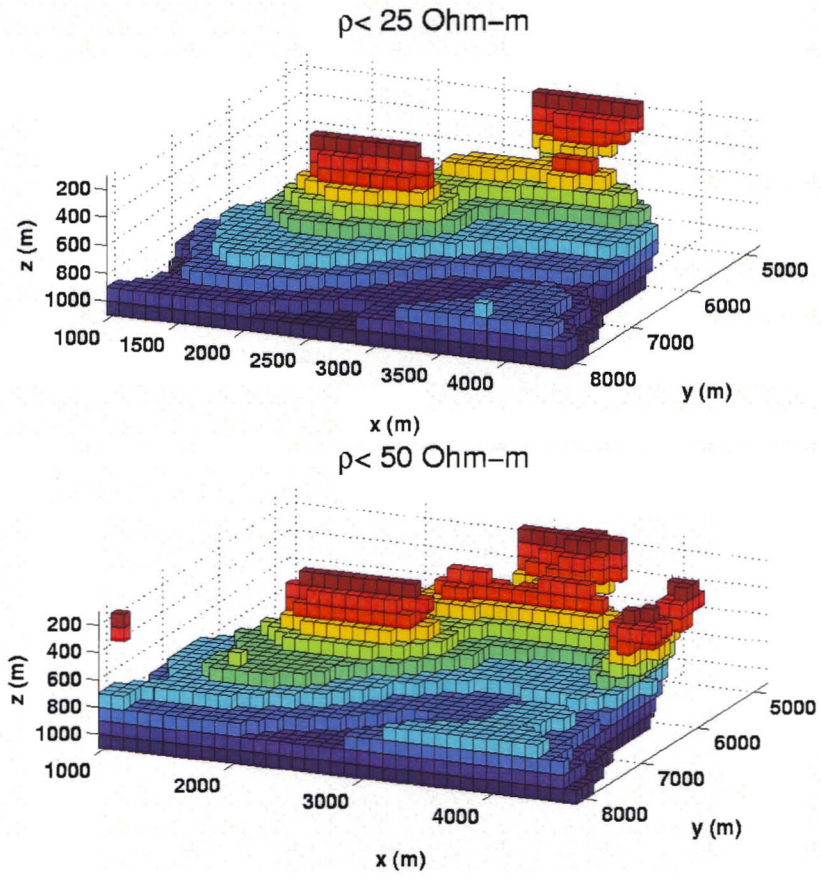

Figure 16: The volume image of the inversion results with resistivity below 25 Ohm-m (upper panel) and below 50 Ohm-m (bottom panel). The color represents the depth of the corresponding cells: the shallow cells are marked by red, while the deep cells are painted in blue.

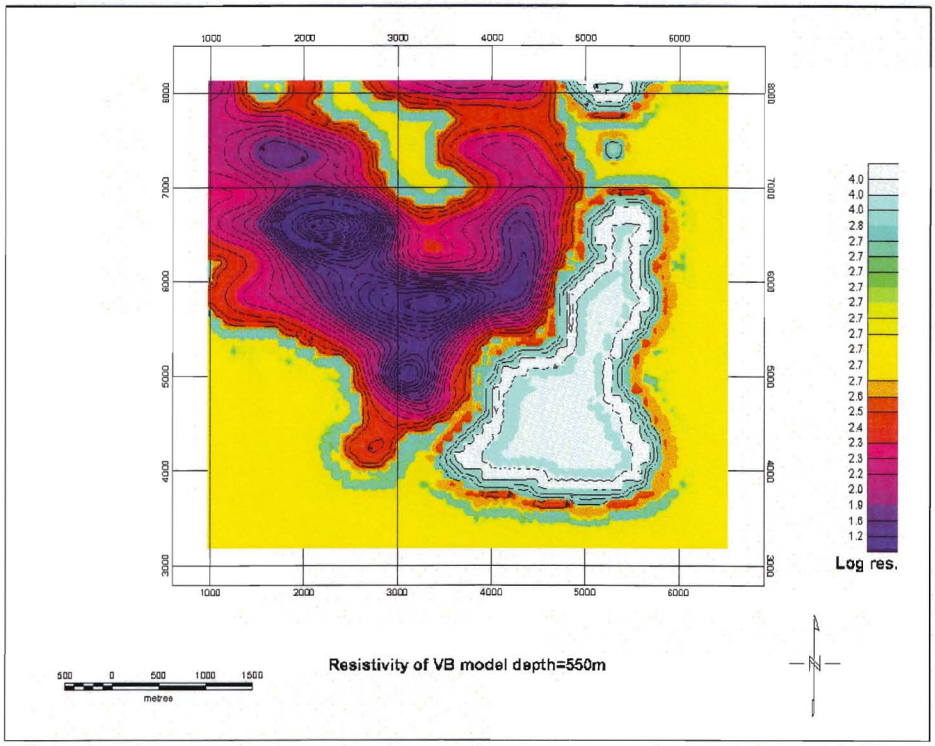

Figure 17: A map of the resistivity distribution at a depth of 550 m, obtained by inversion of the MT data collected in the Voisey's Bay area.

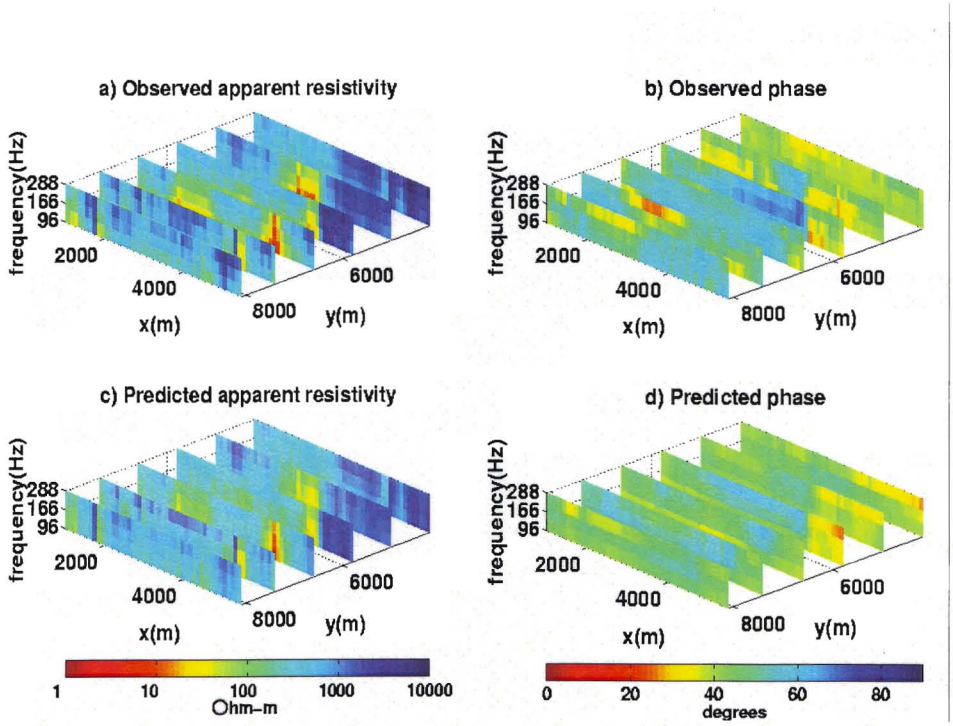

Figure 18: A comparison of the observed and predicted apparent resistivities and phases, computed for the Z_{xy} impedance using the rigorous IE forward modeling code INTEM3D.

It is important to note that, in order to control the accuracy of the inversion, our method allows application of rigorous forward modeling in the intermediate steps of the inversion procedure and for the final inverse model. In particular, we have computed the theoretical predicted MT data for the model shown in Figure 15, using the rigorous forward modeling code INTEM3D. A comparison of the observed and predicted apparent resistivities and phases, computed for the Z_{xy} impedance, is shown in Figure 18a-d. Generally, the apparent resistivities show better agreement than the phases.

Note that the rapid 3-D MT inversion code runs for just about 14 minutes, and the inversion result has been achieved at approximately 30 iterations.

Conclusions

We have developed a new 3-D MT inversion method and computer code based on full nonlinear conjugate gradient inversion and quasi-analytical approximation for the forward modeling solution. Application of the QA approximation for forward modeling and Frechet derivative computations speeds up the calculation dramatically. However, in order to control the accuracy of the inversion, our method allows application of rigorous forward modeling in the intermediate steps of the inversion procedure and for the final inverse model. This modeling is based on the Contraction Integral Equation method developed by Hursan and Zhdanov (2001). The 3-D magnetotelluric inversion code QAINV3D based on QA approximation, developed by CEMI, has been tested on synthetic models and applied to the practical MT data collected in an area with complex geology. This code is based on the re-weighted regularized conjugate gradient method and can produce both smooth and focused images of the geoelectrical structures. The 3-D MT inversion code works extremely fast and produces the reasonable images of subsurface geological formations. The rapid inversion of the array magnetotelluric data (observed with hundreds of multi-frequency observation stations) can be done within a few minutes on a PC to generate the full 3-D image of subsurface formations on a large grid with tens of thousands of cells.

Acknowledgments

The authors acknowledge the support of the University of Utah Consortium for Electromagnetic Modeling and Inversion (CEMI), which includes Baker Atlas Logging Services, BHP Billiton World Exploration Inc., Electromagnetic Instruments, Inc., ExxonMobil Upstream Research Company, INCO Exploration, International Energy Services, Japan National Oil Corporation, MINDECO, Naval Research Laboratory, Rio Tinto-Kennecott, Shell International Exploration and Production Inc., and Sumitomo Metal Mining Co.

Special thanks to INCO Exploration, and in particular to Drs. Alan King and Steve Balch, for providing MT data, collected for mining exploration, and permission to publish the inversion results.

We are thankful also to Dr. Gabor Hursán for his contribution in developing the rapid MT inversion code.

1 References

Balch, S. J., 2000, Geophysics in mineral exploration: fundamentals and case histories. Ni-Cu sulphide deposits with examples from Voisey's Bay: in Practical Geophysics III, Northwest Mining Association.

Berdichevsky, M. N., and V. I. Dmitriev, 2002, Magnetotellurics in the context of the theory of ill-posed problems, Society of Exploration Geophysicists, Tulsa, Oklahoma, 215 pp.

Hursán, G., 2001, Storage reduction and fast matrix multiplication for intergral based geophysical problem: Proceedings of 2001 CEMI Annual Meeting, 17-38.

Hursán, G., and M. S. Zhdanov, 2002, Contraction integral equation method in 3-D electromagnetic modeling: Radio Science, 37, No. 6, 1089.

Mehanee, S., and M. S. Zhdanov, 2002, Two-dimensional magnetotelluric inversion of blocky geoelectrical structures: Journal of Geophys. Research, **107**, No. B4, 10.1029.

Naldrett, A. J., Keats, H., Sparkes, K., and S. Moore, 1996, Geology of the Voisey's Bay Ni-Cu-Co Deposit, Labrador, Canada: Explor. Mining Geol., **5**, 169-179.

Portniaguine O., and M. S. Zhdanov, 1995, Parameter estimation method in the solution of multi-dimensional geo-electromagnetic inverse problems: 3-D electromagnetics: Proceeding of the First International Symposium on Three-Dimensional Electromagnetics, Schlumberger-Doll Research, Ridgefield, CT.

Portniaguine, O. N., and M. S. Zhdanov, 1999, Focusing geophysical inversion images: Geophysics, **64**, 874-887.

Tikhonov, A. N. and V. Y. Arsenin, 1977, Solution of ill-posed problems: V. H. Winston and Sons, Washington D. C.

Wannamaker, P. E., 1999, Affordable magnetotellurics: Interpretation in Natural Environments: in Three-Dimensional Electromagnetics, edited by Michael Oristaglio and Brian Spies, SEG publication.

Zhdanov, M. S., Fang, S., and G. Hursán, 2000a, Electromagnetic inversion using quasi-linear approximation: Geophysics, **65**, 1501-1513.

Zhdanov M. S., Dmitriev, V. I., Fang, S., and Hursán, G., 2000b, Quasi-analytical approximations and series in electromagnetic modeling: Geophysics, **65**, 1746-1757.

Zhdanov, M. S., and G. Hursán, 2000, 3-D electromagnetic inversion based on quasi-analytical approximation: Inverse Problems, **16**, 1297-1322.

Zhdanov, M. S., and G. W. Keller, 1994, The geoelectrical methods in geophysical exploration: Elsevier, Amsterdam-London-New York-Tokyo, 873 pp.

Zhdanov, M. S., 2002, Geophysical Inverse Theory and Regularization Problems: Elsevier, Amsterdam-London-New York-Tokyo, 628 pp.

Appendix A: The matrix form of quasi-analytical approximation

The quasi-analytical approximations (3) and (4) of the anomalous electric and magnetic fields in a discrete form can be written as (Zhdanov, 2002)

$$\mathbf{e}_{QA}^{a} = \widehat{\mathbf{G}}_{E}\hat{\mathbf{e}}_{D}^{b}\left[\mathbf{diag}\left(\mathbf{I}-\mathbf{g}(\boldsymbol{\sigma})\right)\right]^{-1}\boldsymbol{\sigma}, \tag{48}$$

and

$$\mathbf{h}_{QA}^{a} = \widehat{\mathbf{G}}_{H}\hat{\mathbf{e}}_{D}^{b}\left[\mathbf{diag}\left(\mathbf{I}-\mathbf{g}(\boldsymbol{\sigma})\right)\right]^{-1}\boldsymbol{\sigma}. \tag{49}$$

We used the following notations in the last formulae. The vectors $\mathbf{e}_{QA}^{a}$ and $\mathbf{h}_{QA}^{a}$ represent the discrete quasi-analytical approximations of the anomalous electric and magnetic fields at the observation points. Vector $\mathbf{I}$ is a $N\times 1$ column vector whose elements are all unity. The $N\times 1$ column vector $\mathbf{g}(\boldsymbol{\sigma})$ represents the function $g(\mathbf{r})$ (equation (5)) at the center of each cell:

$$\mathbf{g}(\boldsymbol{\sigma}) = \left[\frac{\mathbf{E}^{b,1*}\cdot\mathbf{E}^{B,1}}{\mathbf{E}^{b,1*}\cdot\mathbf{E}^{b,1}}, \frac{\mathbf{E}^{b,2*}\cdot\mathbf{E}^{B,2}}{\mathbf{E}^{b,2*}\cdot\mathbf{E}^{b,2}}, \ldots\ldots, \frac{\mathbf{E}^{b,N*}\cdot\mathbf{E}^{B,N}}{\mathbf{E}^{b,N*}\cdot\mathbf{E}^{b,N}}\right]^{T}, \tag{50}$$

where $\mathbf{E}^{B,j}$ and $\mathbf{E}^{b,j}$ $(j=1,2,...N)$ denote the Born approximation and the background electric field in each cell within the anomalous domain.

Direct calculations show that vector $\mathbf{g}(\boldsymbol{\sigma})$ can be expressed by matrix multiplication:

$$\mathbf{g}(\boldsymbol{\sigma}) = \left(\hat{\mathbf{e}}_{D}^{b}\hat{\mathbf{e}}_{D}^{b*}\right)^{-1}\hat{\mathbf{e}}_{D}^{b*}\mathbf{e}_{D}^{B}, \tag{51}$$

where the vector of the Born approximation inside the anomalous domain, $\mathbf{e}_{D}^{B}$, can be expressed by the formula:

$$\mathbf{e}_{D}^{B} = \widehat{\mathbf{G}}_{D}\hat{\mathbf{e}}_{D}^{b}\boldsymbol{\sigma}. \tag{52}$$

Substituting (52) into (51), we obtain

$$\mathbf{g}(\boldsymbol{\sigma}) = \left(\hat{\mathbf{e}}_{D}^{b}\hat{\mathbf{e}}_{D}^{b*}\right)^{-1}\hat{\mathbf{e}}_{D}^{b*}\mathbf{e}_{D}^{B} = \left(\hat{\mathbf{e}}_{D}^{b}\hat{\mathbf{e}}_{D}^{b*}\right)^{-1}\hat{\mathbf{e}}_{D}^{b*}\widehat{\mathbf{G}}_{D}\hat{\mathbf{e}}_{D}^{b}\boldsymbol{\sigma} = \widehat{\mathbf{C}}\boldsymbol{\sigma}, \tag{53}$$

where

$$\widehat{\mathbf{C}} = \left(\hat{\mathbf{e}}_{D}^{b}\hat{\mathbf{e}}_{D}^{b*}\right)^{-1}\hat{\mathbf{e}}_{D}^{b*}\widehat{\mathbf{G}}_{D}\hat{\mathbf{e}}_{D}^{b}. \tag{54}$$

Thus, we can represent equations (52), (48) and (49) in the form

$$\mathbf{e}^{B} = \widehat{\mathbf{G}}_{E}\hat{\mathbf{e}}_{D}^{b}\boldsymbol{\sigma} = \widehat{\mathbf{A}}_{E}\boldsymbol{\sigma},$$

$$\mathbf{e}^a_{QA}=\widehat{\mathbf{A}}_E\left[\mathbf{diag}\left(\mathbf{I}-\widehat{\mathbf{C}}\boldsymbol{\sigma}\right)\right]^{-1}\boldsymbol{\sigma}=\widehat{\mathbf{A}}_E\hat{\mathbf{B}}(\boldsymbol{\sigma})\,\boldsymbol{\sigma},$$

$$\mathbf{h}^a_{QA}=\widehat{\mathbf{A}}_H\left[\mathbf{diag}\left(\mathbf{I}-\widehat{\mathbf{C}}\boldsymbol{\sigma}\right)\right]^{-1}\boldsymbol{\sigma}=\widehat{\mathbf{A}}_H\hat{\mathbf{B}}(\boldsymbol{\sigma})\,\boldsymbol{\sigma}, \tag{55}$$

where

$$\widehat{\mathbf{A}}_E=\widehat{\mathbf{G}}_E\hat{\mathbf{e}}^b_D,\ \widehat{\mathbf{A}}_H=\widehat{\mathbf{G}}_H\hat{\mathbf{e}}^b_D, \tag{56}$$

and the diagonal matrix is expressed as

$$\hat{\mathbf{B}}(\boldsymbol{\sigma})=\left[\mathbf{diag}\left(\mathbf{I}-\widehat{\mathbf{C}}\boldsymbol{\sigma}\right)\right]^{-1}. \tag{57}$$

Let us introduce a notation $\mathbf{d}$ for an electric or magnetic vector of the anomalous part of the observed data. This vector contains the components of the anomalous electric and/or magnetic fields at the receivers. The discrete forward modeling problem for the electromagnetic field based on the QA approximation can be expressed by the following matrix operations:

$$\mathbf{d}=\widehat{\mathbf{A}}\left[\mathbf{diag}\left(\mathbf{I}-\widehat{\mathbf{C}}\boldsymbol{\sigma}\right)\right]^{-1}\boldsymbol{\sigma}=\widehat{\mathbf{A}}\hat{\mathbf{B}}(\boldsymbol{\sigma})\,\boldsymbol{\sigma}, \tag{58}$$

where $\widehat{\mathbf{A}}$ stands for the electric or magnetic matrices, $\widehat{\mathbf{A}}_E=\widehat{\mathbf{G}}_E\hat{\mathbf{e}}^b_D$ or $\widehat{\mathbf{A}}_H=\widehat{\mathbf{G}}_H\hat{\mathbf{e}}^b_D$, respectively.